

Experimental and Computational Study of a New Wheel-Shaped $\{[W_5O_{21}]_3[(U^{VI}O_2)_2(\mu-O_2)]_3\}^{30-}$ Polyoxometalate

Pere Miró,[†] Jie Ling,[‡] Jie Qiu,[‡] Peter C. Burns,^{‡,§,*} Laura Gagliardi,^{†,*} and Christopher J. Cramer^{†,*}

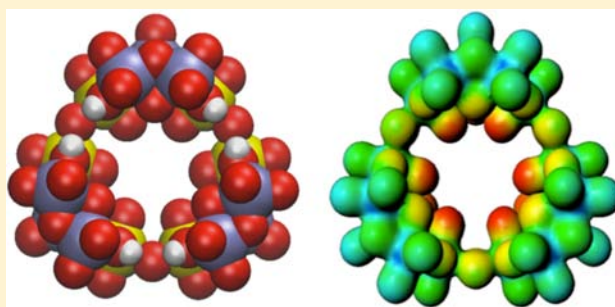
[†]Department of Chemistry and Supercomputing Institute, University of Minnesota, Minneapolis, Minnesota 55455, United States

[‡]Department of Civil Engineering and Geological Sciences, University of Notre Dame, Notre Dame, Indiana 46556, United States

[§]Department of Chemistry and Biochemistry, University of Notre Dame, Notre Dame, Indiana 46556, United States

S Supporting Information

ABSTRACT: A new wheel-shaped polyoxometalate $\{[W_5O_{21}]_3[(U^{VI}O_2)_2(\mu-O_2)]_3\}^{30-}$ has been synthesized and structurally characterized. The calculated electrostatic potential reveals the protonation of several μ -oxo bridges reducing the polyoxometalate total charge. A protonated structure computed at the density functional level of theory (DFT) is in good agreement with the experimental fit. This species presents a classical polyoxometalate electronic structure with well-defined metal and oxo bands belonging to its U/W and oxo/peroxo constituents, respectively. Furthermore, fragment calculations indicate that the electronic structures of the uranyl–peroxide and polyoxotungstate fragments are little affected by the nanowheel assembly.



1. INTRODUCTION

The first known observation of polyoxometalates (POMs) dates from centuries ago when Native Americans observed a mysterious blue water in Idaho Springs and in the Valley of Ten Thousand Smokes.^{1,2} It is now thought that this coloration was due to the molybdenum blue in solution that formed naturally upon the partial oxidation of molybdenite (MoS_2). However, POM chemistry started long after, with Berzelius,³ and since then many eminent researchers such as Werner, Pauling, and Pope have unveiled the structure, reactivity, and properties behind these species.^{4–7}

Nowadays, POMs are a wide family of discrete metal–oxygen inorganic molecules with a range of applications ranging from catalysis to medicine.⁸ It is remarkable that, during the nearly two centuries of POM chemistry, almost all of the elements of the periodic table have somehow been incorporated into a POM framework revealing their wide structural variety.⁴ However, despite this structural diversity, there are few well-characterized POMs containing uranium. In the late 1990s, Kim et al.⁹ reported the first tungstophosphate containing two uranyl moieties, $[Na_2(U^{VI}O_2)_2(PW_9O_{34})_2]^{12-}$. After this breakthrough into the synthesis of POMs with uranium, Pope's group reported many similar uranium-containing tungstometalates such as $[Na_2(U^{VI}O_2)(GeW_9O_{34})_2]^{14-}$, $[(Na(H_2O))_4(U^{VI}O_2)_4(SiW_{10}O_{34})_4]^{22-}$, $[(U^{VI}O_2)_3(H_2O)_6As_3W_{30}O_{105}]^{15-}$, and $[(U^{VI}O_2)_{12}(\mu^3-O)_4(\mu^2-H_2O)_{12}(P_2W_{15}O_{56})_4]^{32-10-13}$. Furthermore, the first lanthanide derivatives with general formula $Ln_4(H_2O)_{28}[K@P_8W_{48}O_{184}(H_4W_4O_{12})_2Ln_2(H_2O)_{10}]^{13-}$ ($Ln = La, Ce, Pr, Nd$) were also prepared in Pope's group.¹⁴

In 2005, we reported the self-assembly of a new family of uranyl and neptunyl peroxide nanoclusters in alkaline solutions under ambient conditions.¹⁵ Whereas uranyl minerals and synthetic compounds generally adopt extended structures based upon sheet structural units, the inclusion of peroxo bridges between actinide ions fosters the formation of nanoscale cage clusters.¹⁶ Further studies have extended the family of uranyl peroxo cage clusters to more than 30 nanoclusters with diverse bridging ligands between the uranyl moieties such as peroxide, hydroxyl, pyrophosphate, or oxalate.^{17–25} Recently, these species have demonstrated their potential importance in nuclear accidents.²⁶

During the last years, several uranyl–peroxide nanoclusters' building blocks have been identified.^{27–31} Among these, Sigmon et al.³¹ isolated one of the smallest known building blocks formed by two uranyl ions and a bridging bidentate peroxo ligand (Figure 1). Recently, DFT and complete active space self-consistent field (CASSCF) calculations have been used to study the electronic structure and bonding of this species.^{27,28}

The first uranyl–peroxide tungstometalate $LiK_4\{(U^{VI}O_2)_4(\mu-O_2)_4(H_2O)_2\}_2(PO_3OH)_2P_6W_{36}O_{136}\}^{25-}$ was reported by Mal et al.³² This species has two well-defined building blocks: $[(U^{VI}O_2)_4(\mu-O_2)_4]$ uranyl–peroxide and $[P_2W_{12}]^{10-}$ tungstometalate fragments. We are currently interested in the interaction of d transition-metal polyoxometalates and actinides in basic peroxide bearing environments.

Received: March 14, 2012

Published: August 2, 2012

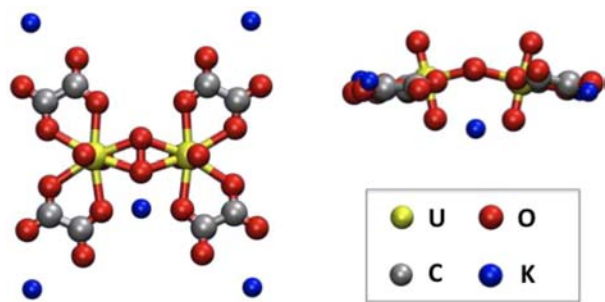


Figure 1. Top and side view of the X-ray structure of the uranyl peroxide dimer, $K_5[(U^{VI}O_2)_2(\mu-O_2)(C_2O_4)_4]^-$, synthesized by Sigmon et al.³¹

In this Article, we present the synthesis and characterization of a wheel-shaped $\{[W_5O_{21}]_3[(U^{VI}O_2)_2(\mu-O_2)]_3\}^{30-}$ (designated U_6W_{15}) polyoxometalate that is formed by well-defined $[(U^{VI}O_2)_2(\mu-O_2)]^{2+}$ dimers and $[W_5O_{21}]^{12-}$ tungstometalate fragments. A DFT study and topological analysis of the electron density give insights into the electronic structure and bonding of this species.

2. EXPERIMENTAL SECTION

2.1. Materials. Although isotopically depleted uranium was used for all experiments described here, appropriate precautions are essential for handling all toxic and radioactive materials. $U^{VI}O_2(NO_3)_2 \cdot 6H_2O$ (MV Laboratories, Lot no. P705UA1), H_2O_2 (30%, Alfa-Aesar), $LiOH \cdot H_2O$ (98%, Sigma-Aldrich), $H_3PW_{12}O_{40}$ (10%, Sigma-Aldrich), $NaOH$ (99%, Sigma-Aldrich), were used as received. Distilled and Millipore filtered water with a resistance of 18.2 $M\Omega$ cm was used in all reactions.

2.2. Synthetic Procedure. Crystals containing the $Na_6Li_{24}\{[W_5O_{21}]_3[(U^{VI}O_2)_2(\mu-O_2)]_3\}$ cluster were synthesized by slow evaporation of mixed solutions containing 0.1 mL $U^{VI}O_2(NO_3)_2$ (0.5 M), 0.1 mL H_2O_2 (30%), 0.1 mL $LiOH$ (2.38 M), 0.15 mL phosphotungstic acid (10%), and 0.1 mL $NaOH$ (0.1 M) that had an initial pH of 8.8. Yellow prism-shaped crystals appeared after two months of solution aging under ambient conditions with the solutions opened to air. The crystal yield was 8% based on uranium.

2.3. X-ray Crystallography. X-ray diffraction data was collected at 110 K using a Bruker goniometer, an APEX II CCD detector, and graphite-monochromated $MoK\alpha$ radiation from a conventional tube. A correction for absorption was applied to the full sphere of data using the program *SADABS*. Data were integrated using the Bruker *APEX II* software and the *SHELXTL*³³ system of programs was used for the solution and refinement of the structure. Selected crystallographic data are presented in Table 1.

2.4. Inductively Coupled Plasma Spectroscopy (ICP). Crystals of $Na_6Li_{24}\{[W_5O_{21}]_3[(U^{VI}O_2)_2(\mu-O_2)]_3\}$ were washed lightly with deionized water under vacuum and were subsequently dissolved for analysis using a PerkinElmer ICP-OES. Analysis for three separately washed samples gave a consistent U/W/Na/Li ratio of 6:16:6:24.

2.5. Infrared Spectroscopy (IR). Infrared spectra were collected from a single crystal of $Na_6Li_{24}\{[W_5O_{21}]_3[(U^{VI}O_2)_2(\mu-O_2)]_3\}$ using a SensIR technology IlluminatIR FTIR microspectrometer. A single crystal was placed on a glass slide, and the spectrum was collected using a diamond ATR objective from 650 to 4000 cm^{-1} with a beam aperture of 100 μm .

Table 1. Summary of Crystallographic Data for $Na_6Li_{24}\{[W_5O_{21}]_3[(U^{VI}O_2)_2(\mu-O_2)]_3\}$

compound	U_6W_{15}
empirical formula	$Na_6Li_{24}U_6W_{15}O_{81}$
fw	5786.199
temperature (K)	110
wavelength (\AA)	0.71073
cryst syst	triclinic
space group	P1
<i>a</i> (\AA)	18.675(3)
<i>b</i> (\AA)	25.903(5)
<i>c</i> (\AA)	29.294(5)
α ($^\circ$)	65.962(2)
β ($^\circ$)	97.062(2)
γ ($^\circ$)	85.706(2)
<i>V</i> (\AA^3)	12902(4)
<i>Z</i>	4
density ($g \cdot cm^{-3}$)	3.147
<i>M</i> (mm^{-1})	20.920
<i>F</i> ₀₀₀	10500
goodness-of-fit on <i>F</i> ²	1.046
<i>R</i> ₁ ^a [<i>I</i> > 2 σ (<i>I</i>)]	0.1383
<i>wR</i> ₂ ^b	0.3574

$$^a R_1 = \sum ||F_o| - |F_c|| / \sum |F_o|. \quad ^b wR_2 = \sum [w(F_o^2 - F_c^2)^2] / \sum [w(F_o^2)^2]^{1/2}.$$

2.6. Thermal Gravimetric Analysis (TGA). A Thermal Gravimetric Analysis measurement was conducted using a Netzsch TG209 F1 Iris thermal analyzer for 18 mg of crystalline $Na_6Li_{24}\{[W_5O_{21}]_3[(U^{VI}O_2)_2(\mu-O_2)]_3\}$ in an Al_2O_3 crucible that was heated from 20 to 900 $^\circ C$ at a rate of 5 $^\circ C/min$ under flowing nitrogen gas.

2.7. Computational Details. All calculations were performed using the *Amsterdam Density Functional (ADF2010)* program developed by Baerends et al.³⁴ and the Becke88-Perdew86 (BP86) exchange-correlation functional.^{35–37} Relativistic corrections were introduced by the scalar-relativistic zero-order regular approximation (ZORA).^{38,39} A triple- ζ plus polarization basis set was used on all atoms. For non-hydrogen atoms a relativistic frozen-core potential was used. Solvent effects (aqueous) were introduced in the geometry optimization by using the COSMO continuum solvation model with standard Allinger radii^{40–42} except for the alkali counterions for which radii reproducing experimental free energies of aqueous solvation were used.^{43,44} An integration parameter of 4.5 was used except for frequency calculations where the parameter was set to 6.0.

This computational procedure has been widely used in the study of classical polyoxometalates^{45–48} and polyperoxouranates⁴⁹ and the use of scalar ZORA to treat the relativistic effects is a standard procedure in late transition metals, actinides, and lanthanides.⁵²

Analytical vibrational frequencies showed small imaginary frequencies corresponding to reorientations of protons on the $\mu-OH$ moieties away from the symmetry (D_{3h}) imposed in all of the calculations. Single-point calculations were performed using the same computational protocol but with the LB94, PBE, and M06-L functionals in order to study their effects on the POM electronic structure.^{50,51} The geometry was also reoptimized using the M06-L functional.

A single-point calculation to generate a WFN file was performed using the *TURBOMOLE* 6.3.1 package⁵³ with the Becke88-Perdew86 (BP86)^{35–37} exchange-correlation func-

tional and triple- ζ valence plus polarization (def-TZVP) basis sets on all atoms.⁵⁴ A small-core quasi-relativistic pseudopotential was used for uranium. The resolution of the identity (RI) approximation was used to speed the calculation of the Coulomb integrals.^{55–57} Solvation effects associated with water as solvent were accounted for using the COSMO continuum solvation model.⁵⁸ Topological analysis of the electron density was performed with the *Multiwfn* 2.2.1 package developed by Lu et al.⁵⁹

3. RESULTS AND DISCUSSION

3.1. U_6W_{15} Structure. Solution of the structure based on the single-crystal X-ray diffraction data provided the locations of the uranium atoms, tungsten atoms, and the oxygen atoms that coordinate both. Two Na^+ sites were located. Li^+ and H^+ cations were not located in the difference-Fourier maps because of their low X-ray scattering efficiencies. The structure contains large areas with significant electron density that we attribute to disordered Na^+ , Li^+ , and H_2O . ICP-OES analyses indicate 6 Na^+ and 24 Li^+ cations charge-balance the U_6W_{15} cluster in the crystal.

The TGA measurement shows a 32% weight loss over the temperature range of 25 to 900 °C (Figure 2). The initial

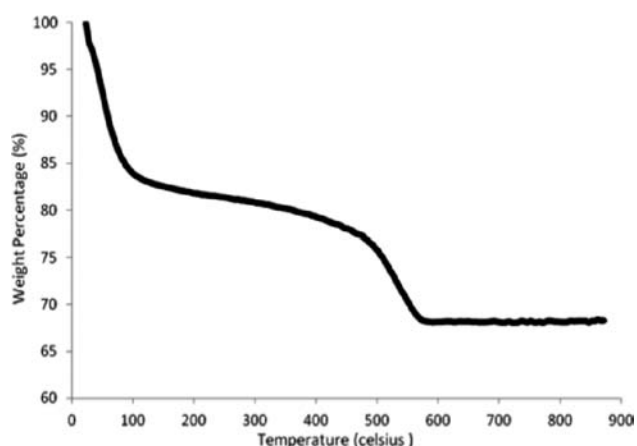


Figure 2. Thermal gravimetric analysis profile for U_6W_{15} .

weight loss by 100 °C of about 17% is likely due to loss of solvent water. Subsequent weight loss is likely due to breakdown of peroxide and loss of alkali cations. The structure

determination and compound characterization indicate the composition $Na_6Li_{24}\{[W_5O_{21}]_3[(U^{VI}O_2)_2(\mu-O_2)]_3\}(H_2O)_{50}$.

All U^{VI} cations are present as typical $[U^{VI}O_2]^{2+}$ uranyl ions with U–O bond lengths of ca. 1.8 Å and O=U=O bond angles of ca. 180°. The uranyl ions are coordinated by six ligands arranged at the equatorial vertices of hexagonal bipyramids in which the apexes are defined by the O atoms of the uranyl ion. The equatorial ligands of the uranyl hexagonal bipyramids consist of a bidentate peroxide group and four oxygen atoms that bridge to W. The equatorial U–O bond distances range from 2.21 to 2.56 Å. Two uranyl polyhedra are bridged by a peroxide group, giving a $[(U^{VI}O_2)_2(\mu-O_2)]^{2+}$ dimer. The U–(O₂)–U dihedral angles range from 141.5 to 147.1°, consistent with reported uranyl peroxide clusters.^{15,31} The W cations are either coordinated by five O atoms in a square pyramidal arrangement or by six O atoms in an octahedral arrangement. W–O bond distances range from 1.69 to 2.42 Å. Four WO_6 octahedra and one WO_5 square pyramid are linked through shared vertices to give a five-membered tungstate fragment with composition $[W_5O_{21}]^{12-}$. A bond-valence analysis of the refined structure showed that some of the O atoms in the cluster have bond-valence sums near their formal valence when only the W–O and U–O bonds are considered. However, other O atoms have bond-valence sums that are well below their formal valences. This may be due to protonation, or to bonds to Na^+ or Li^+ cations that we have not accounted for because these cations are disordered outside the clusters. Therefore, we do not identify protonation sites from the X-ray data but rather address this from a computational perspective. The WO_5 unit is surrounded by WO_6 octahedra, and each of the equatorial vertices of the square pyramid is shared with one octahedron. Pairs of octahedra share an edge, and each uranyl hexagonal bipyramid shares three of its equatorial edges with the $[W_5O_{21}]^{12-}$ fragment – two with WO_6 octahedra and one with a WO_5 square pyramid. Three dimers of uranyl peroxide polyhedra and three $[W_5O_{21}]^{12-}$ tungstate fragments are linked to form the ring-shaped U_6W_{15} (Figure 3). The U_6W_{15} is 14.7 by 6.4 Å in diameter as measured from the outer and inner edges of bounding O atoms. Two well-ordered Na^+ cations were located in the structure. These are outside the U_6W_{15} cluster and are five- or six-coordinated by tungstate O atoms and H_2O groups and link the U_6W_{15} rings (cif file in the Supporting Information).

The calculated U_6W_{15} structure compares to the experimental structure with an average deviation of ca. 0.05 Å in

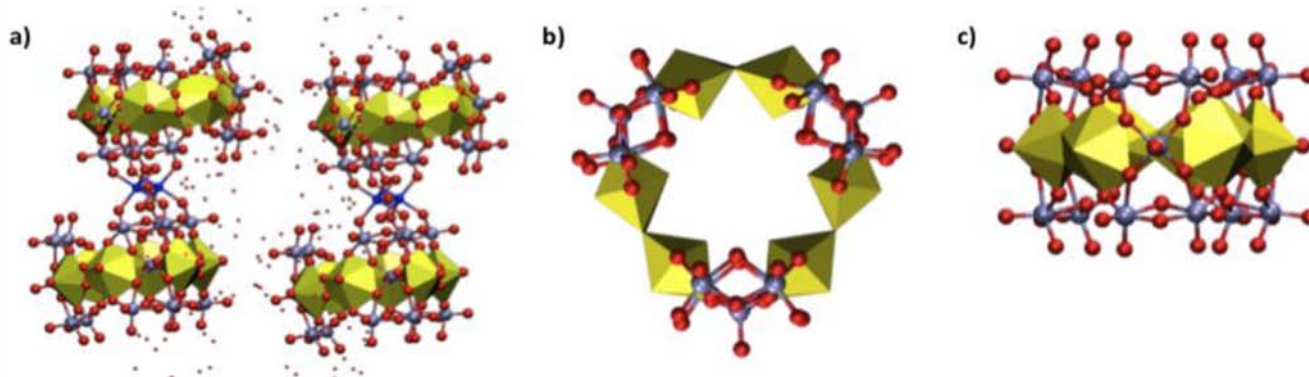


Figure 3. (a) Crystal packing of four $Na_6Li_{24}\{[W_5O_{21}]_3[(U^{VI}O_2)_2(\mu-O_2)]_3\}$ (U_6W_{15}). Lithium atoms were not located in the crystal structure. (b) Top view of one U_6W_{15} structure. (c) Side view of one U_6W_{15} structure. In all cases uranyl–peroxide and tungstometalate fragments are shown in polyhedral and ball and stick representations, respectively. Color code: Tungsten in ice blue, potassium in deep blue and uranium in yellow.

Table 2. Selected Experimental and Computed Geometrical Parameters (in Angstroms and Degrees) for U_6W_{15} , $Na_3U_6W_{15}$, and $H_{18}U_6W_{15}$ Compared with Other Uranyl–Peroxide and Polyoxometalate Species; Calculated Parameters at BP86 Level of Theory (M06-L in Parentheses)

	U_6W_{15}		$Na_3U_6W_{15}$	$H_{18}U_6W_{15}$	U_2^a	U_{20}^b		Pope et al. ^c	Kortz et al. ^d
	X-ray	DFT	DFT	DFT	X-ray	X-ray	DFT	X-ray	X-ray
U=O _{term.}	1.79	1.860 (1.825)	1.859	1.829 (1.800)	1.788	1.810	1.860	1.785	1.821
U–O _{perox.}	2.37	2.423 (2.397)	2.478	2.377 (2.385)	2.336	2.330	2.380		2.350
O _{perox.} –O _{perox.}	1.46	1.460 (1.450)	1.463	1.454 (1.459)	1.473	1.530	1.480		1.480
U–O _{bridge-W}	2.42	2.381 (2.412)	2.347	2.493 (2.491)				2.343	2.331
W=O _{term.}	1.76	1.839 (1.805)	1.836	1.774 (1.774)				1.748	1.719
W–O _{bridge-U}	1.84	1.903 (1.862)	1.914	2.052 (2.038)				1.829	1.815
W–O _{bridge-W}	2.09	2.050 (2.013)	2.037	2.109 ^e (2.086)				1.961	1.863
W ₂ –O–U ^f	2.17	2.222 (2.201)	2.230	2.195 (2.192)				2.157	
U–(O ₂)–U	144.3	144.4 (143.1)	168.9	141.5 (151.3)	153.0	139.0	142.1		133.5

^a $K_5[(U^{VI}O_2)_2(O_2)(C_2O_4)_4]^-$. Ref 31. ^b $Na_{12}[(U^{VI}O_2)_{20}(O_2)_{30}]^{8-}$. Refs 31 and 63. ^c $[Na_2(U^{VI}O_2)_2(PW_9O_{34})_2]^{12-}$. Ref 9. ^d $LiK_4[(U^{VI}O_2)_4(O_2)_4(H_2O)_2(PO_3OH)_2P_6W_{36}O_{136}]^{25-}$. Ref 32. ^eAverage between μ -oxo and μ -hydroxo moieties. ^fAverage between three non equivalent bonds.

bond distances and 0.1° with respect to the average U–O₂–U dihedral angle (Table 2). The large negative charge of POMs in general, and analogously the U_6W_{15} species, is partially compensated through the protonation of bridging oxos and/or formation of ion pairs with the counterions present in the media.⁶¹ The electrostatic potential has been demonstrated to be a reliable indicator of the protonation sites on classical POMs and uranyl–peroxide nanocapsules.^{62,63} The U_6W_{15} electrostatic potential is presented in the top of Figure 4 revealing that the negative charge is more localized on internally directed O atoms including both uranyl terminal oxygens and μ -oxo ligands between tungstens and tungsten–uranium centers. It is well-known that uranyl moieties are rarely protonated and they usually interact with the alkali counterions present in the media.^{27,28,31,55} Three sodium counterions were

included under the uranyl oxygens pointing toward the center of the ring, $Na_3\{[W_5O_{21}]_3[(U^{VI}O_2)_2(\mu-O_2)]_3\}^{27-}$ ($Na_3U_6W_{15}$). The nanowheel bond distances are almost unaffected by the presence of the counterions, however the U–(O₂)–U dihedral angles flatten to 168.9° (Table 2).³¹ This dihedral has been identified to be highly flexible and affected by the presence of alkali counterions in previous studies. Consequently, it appears unlikely that an alkali counterion is located under the uranyl moieties of U_6W_{15} species. An alternative to reduce the total charge of this species is the protonation of the internal μ -oxo ligands such as W–O_{bridge}–W and W–O_{bridge}–U that will be in agreement with the well established higher basicity of the bridging oxos in POMs.⁴ Indeed, the geometry of the protonated $H_{18}\{[W_5O_{21}]_3[(U^{VI}O_2)_2(\mu-O_2)]_3\}^{12-}$ ($H_{18}U_6W_{15}$) species is also in agreement with the X-ray structure with an average error in bond distances of 0.04 Å and 2.9° with respect to the average U–O₂–U dihedral angle (Table 2). This demonstrates that the U_6W_{15} protonation has almost no effect on its structure. Furthermore, the electrostatic potential of $H_{18}U_6W_{15}$ shows that now the charge is more distributed among the nanowheel structure but still the uranyl oxygens are the more negative centers (bottom of Figure 4). No significant changes in the structure were observed when single points were performed with other functionals or when the structures were reoptimized at the M06-L level of theory (Supporting Information for details).

3.2. Infrared Spectra. The IR spectrum for the U_6W_{15} species is presented in Figure 5. Bands are assigned based on available spectroscopic data for POMs and uranyl–containing species and the calculated spectrum for $H_{18}U_6W_{15}$.⁶ The bands at 666 and 676 cm^{-1} are assigned to the protonated μ -oxos bridging between the tungsten centers.⁶⁴ The band at 844 cm^{-1} is assigned to the protonated μ -oxos bridging between the uranium and tungsten centers. The peak at 971 cm^{-1} is assigned to W=O stretching bands, and the band at 760 cm^{-1} is assigned to the symmetric stretch of the uranyl U=O bonds, whereas the corresponding asymmetric stretch is likely hidden under the W=O band. The broad band at 3100–3400 cm^{-1} can be assigned to interstitial water and/or to protonated μ -oxo bridging ligands in the U_6W_{15} structures.⁶⁵ See the Supporting Information for calculated spectra.

3.3. Electronic Structure. The U_6W_{15} species presents an expected polyoxometalate electronic structure with *Sf* uranium and *d* tungsten orbitals composing the first set of empty energy

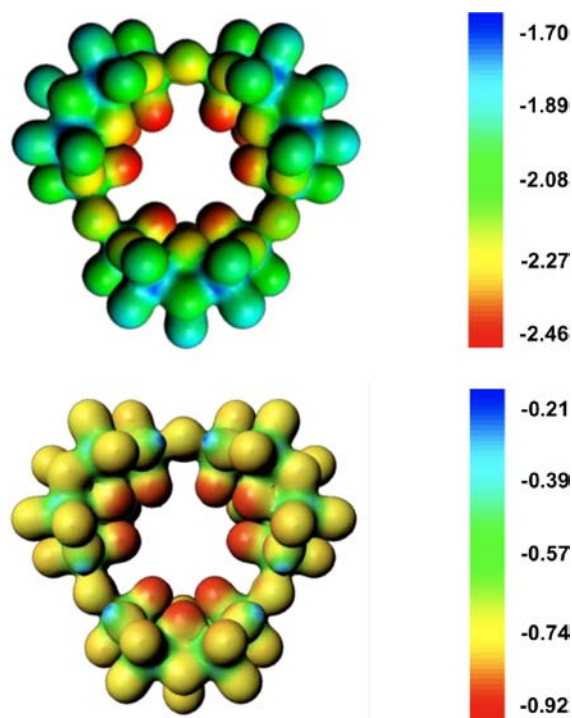


Figure 4. Electrostatic potential plot for the U_6W_{15} (top) and $H_{18}U_6W_{15}$ (bottom) species.

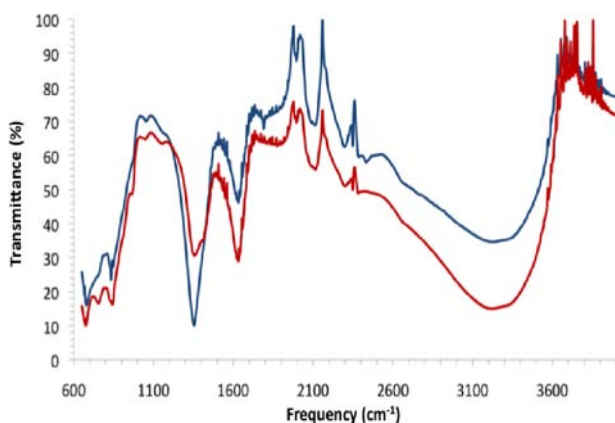


Figure 5. Experimental infrared spectrum of two samples of U_6W_{15} synthesized independently.

levels (metal band), whereas the highest occupied orbitals belong to the oxo and peroxo moieties (oxo/peroxo band). These bands can be easily identified in the density of states (DOS) and selected molecular orbitals of U_6W_{15} presented in Figure 6.

The highest occupied frontier orbitals are localized on the peroxo ligands (HOMO to HOMO-2) and involve antibonding combinations of the peroxo π^* orbitals with small bonding contributions from the uranium centers. Lower in energy is the top of the tungstometalate-oxo band (e.g., HOMO-3). The metal band is formed by empty *f* uranium orbitals (LUMO) and the first empty *d* tungsten orbital is quite high in energy (LUMO+21).^{27,63} A fragment analysis was carried out and reveals that the U_6W_{15} wheel orbitals assemble in an almost unperturbed fashion from constituent uranyl-peroxide and tungstometalate fragments (Supporting Information for details). The electronic structure of the $H_{18}U_6W_{15}$ species is analogous to that of the unprotonated species.

This electronic structure conforms with previous theoretical studies on similar systems.^{27,28,63} Our calculations indicate that these species can be classified as a particular subclass of

polyoxometalates in which the metal ligands are not only oxos (O^{2-}) but also peroxos (O_2^{2-}). This has a direct impact on the growth, structural shape, and stability these species. One example of the latter is that the reduction of the uranyl-peroxide nanocapsules is expected to be irreversible, in contrast with traditional POM redox properties. The presented frontier orbitals indicate that the reduction of this species occurs via a U^{VI}/U^V reduction. Subsequently, U^V disproportionation could lead to the degradation of the bridging peroxide in the $[(U^{VI}O_2)_2(\mu-O_2)]^{2+}$ fragment and consequently an irreversible degradation of the nanowheel structure.

3.4. Topological Electron Density Analysis. To study the character of the chemical bonds involved in U_6W_{15} and the protonated $H_{18}U_6W_{15}$ systems, we analyzed the topology of the electron density within the quantum theory of atoms in molecules (AIM) developed by Bader,^{66,67} which establishes criteria for the identification of bonds, atoms, and atomic arrangements like rings or cages.

A chemical bond exists if a line of a locally maximum electron density links two neighboring atoms and along that line there is a bond critical point (BCP; $\Delta\rho = 0$). At a BCP, the Laplacian of the electron density may be either positive or negative because it is the sum of two negative and one positive eigenvalues of the density Hessian matrix. A positive Laplacian means a local depletion of charge, whereas a negative value is a sign of a local concentration of charge. The latter is observed in covalent bonds because a negative Laplacian indicates a shared interaction of electron density between two atoms; meanwhile a positive Laplacian is consistent with a more ionic bond due to depletion of charge at the location of the BCP. We follow the bond classification depending on the total electronic energy density (E_b^e) at the BCP as suggested by Bianchi et al.⁶⁸ The E_b^e is defined as the sum of the kinetic energy density (G_b) and the potential energy density (V_b) that is usually negative. The first term usually dominates in a noncovalent bond and the second is associated with accumulation of charge between the nuclei (covalent bond).

All of the intuitively expected bonds in U_6W_{15} are characterized by bond critical points, for example the peroxide

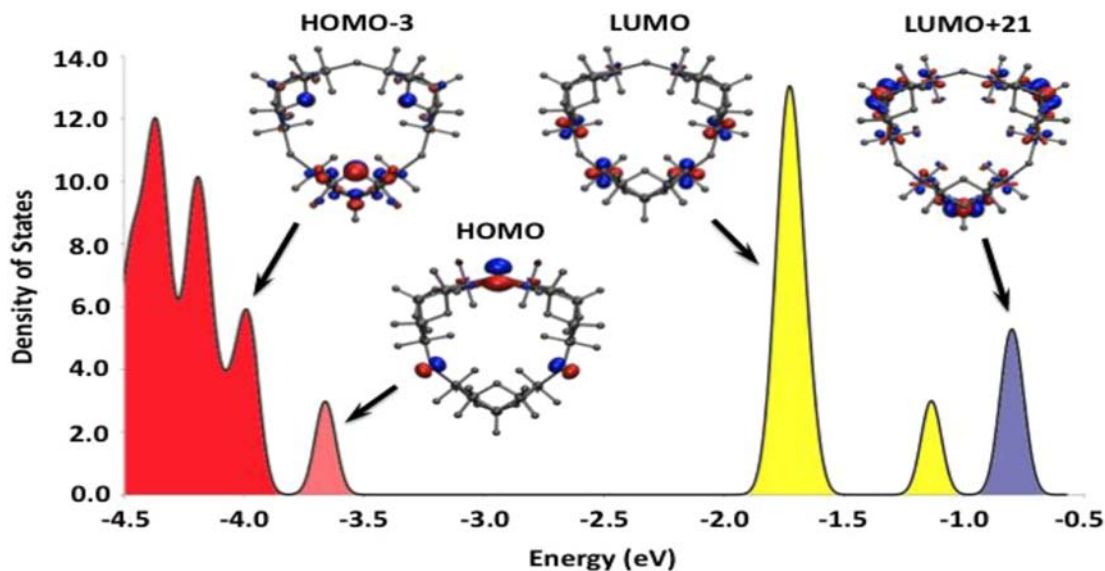


Figure 6. DOS and selected molecular orbitals for U_6W_{15} . In red the oxo band (O^{2-}), in light red the peroxo band (O_2^{2-}), in yellow the uranium metal band (*f* orbitals), and in purple the tungsten metal band (*d* orbitals).

Table 3. Theoretical Bond Critical Point (BCP) Properties for the U_6W_{15} Species, All Values Are Expressed in Atomic Units

type	location	ρ_b	$\nabla^2\rho_b$	G_b	V_b	E_b^e
bond critical point	$O_{\text{uranyl}}-O_{\text{uranyl}}$	0.00400	0.01340	0.00260	-0.00184	0.00075
bond critical point	$U-O_{\text{perox}}$	0.06339	0.19379	0.05914	-0.69833	-0.63919
bond critical point	$O_{\text{perox}}-O_{\text{perox}}$	0.26426	0.20149	0.20799	-0.36561	-0.15762
ring critical point	$O_{\text{uranyl}}-O_{\text{uranyl}}$	0.00374	0.01270	0.00252	-0.00186	0.00066
ring critical point	$U-(O_{\text{perox}})_2$	0.05062	0.24532	0.06389	-0.06645	-0.00257

oxygen–oxygen and the uranyl–peroxide bonds. In each of these instances, the BCPs have negative values of E_b , in agreement with a covalent nature of the bonds. Interestingly, by this analysis the uranyl–peroxide bond is more covalent than the oxygen–oxygen peroxide bond because $E_b(U-O_{\text{perox}}) < E_b(O_{\text{perox}}-O_{\text{perox}})$.

Analogously, topological analysis of the electron density reveals the presence of ring critical points (RCP) in the center of uranium–peroxide triangles/rings. Finally, a BCP and a RCP can be found between the internal uranyl oxygens; however, their electron densities at their critical points are 1 order of magnitude lower than those presented up to now. In consequence, is it not probable that these bonds are sufficient to disrupt ion complexation of these oxygens with alkali counterions or to influence $U-(O_2)-U$ bending. No significant change in the above analysis is observed for the topological of the electron density associated with $H_{18}U_6W_{15}$ (Supporting Information).

4. CONCLUSIONS

In conclusion, we have synthesized a new wheel-shaped polyoxometalate containing two well-defined uranyl–peroxide and tungstometalate building blocks. The U_6W_{15} nanostructure has been structurally characterized by X-ray diffraction and IR spectroscopy. Alkali counterions Li^+ and Na^+ are not complexed with the uranyl moieties as has been observed in other uranyl–peroxide nanocapsules. Instead, calculated electrostatic potentials reveal probable protonation of several μ -oxo bridges to reduce the polyoxometalate total charge. Protonation of these centers has no significant effect on the nanowheel structure. From an electronic structure viewpoint, U_6W_{15} presents a classical POM electronic structure with well-defined metal and oxo bands belonging to its U/W and oxo/peroxo constituents, respectively.

■ ASSOCIATED CONTENT

Supporting Information

X-ray structure, DFT optimized structures, IR spectra, Bader analysis details, and molecular orbitals. This material is available free of charge via the Internet at <http://pubs.acs.org>.

■ AUTHOR INFORMATION

Corresponding Author

*E-mail: cramer@umn.edu (C.J.C.), gagliardi@umn.edu (L.G.), pburns@nd.edu (P.C.B.).

Author Contributions

The manuscript was written through contributions of all authors. All authors have given approval to the final version of the manuscript.

Notes

The authors declare no competing financial interest.

■ ACKNOWLEDGMENTS

This material is based upon work supported as part of the Materials Science of Actinides Center, an Energy Frontier Research Center funded by the U.S. Department of Energy, Office of Science, Office of Basic Energy Sciences under Award Number DE-SC0001089. C.J.C. thanks the U.S. National Science Foundation (CHE09-52054).

■ REFERENCES

- (1) Müller, A.; Serain, C. *Acc. Chem. Res.* **2000**, *33*, 2.
- (2) *Gmelins Handbuch der Anorganischen Chemie*. Verlag Chemie: Berlin, 1935; Vol. 53.
- (3) Berzelius, J. J. *Poggendorffs Annalen der Physik und Chemie* **1826**, *6*, 369.
- (4) Pope, M. T. *Heteropoly and Isopoly Oxometalates*; Springer-Verlag: New York, 1983.
- (5) Special Issue, *Chem. Rev.* **98**, 1-390. **1998**.
- (6) Moffat, J. B. *Metal-Oxygen Clusters: The Surface and Catalytic Properties of Heteropoly Oxometalates*; 1 ed.; Springer: New York, 2001.
- (7) Pope, M. T.; Müller, A. *Polyoxometalate Chemistry: From Topology Via Self-Assembly to Applications*; Kluwer Academic Publishers: Netherlands, 2001.
- (8) Katsoulis, D. E. *Chem. Rev.* **1998**, *98*, 359.
- (9) Kim, K. C.; Pope, M. T. *J. Am. Chem. Soc.* **1999**, *121*, 8512.
- (10) Kim, K. C.; Pope, M. T. *J. Chem. Soc., Dalton Trans.* **2001**, 986.
- (11) Kim, K. C.; Gaunt, A.; Pope, M. T. *J. Cluster Sci.* **2002**, *13*, 423.
- (12) Gaunt, A. J.; May, I.; Copping, R.; Bhatt, A. I.; Collison, D.; Fox, O. D.; Holman, K. T.; Pope, M. T. *Dalton Trans.* **2003**, 3009.
- (13) Khoshnavazi, R.; Eshtiagh-Hossieni, H.; Alizadeh, M. H.; Pope, M. T. *Polyhedron* **2006**, *25*, 1921.
- (14) Zimmermann, M.; Belai, N.; Butcher, R. J.; Pope, M. T.; Chubarova, E. V.; Dickman, M. H.; Kortz, U. *Inorg. Chem.* **2007**, *46*, 1737.
- (15) Burns, P. C.; Kubatko, K. A.; Sigmon, G.; Fryer, B. J.; Gagnon, J. E.; Antonio, M. R.; Soderholm, L. *Angew. Chem., Int. Ed.* **2005**, *44*, 2135.
- (16) Burns, P. C.; Hughes, K. A. *Am. Mineral.* **2003**, *88*, 1165.
- (17) Ling, J.; Qiu, J.; Burns, P. C. *Inorg. Chem.* **2012**, *51*, 2403.
- (18) Sigmon, G. E.; Burns, P. C. *J. Am. Chem. Soc.* **2011**, *133*, 9137.
- (19) Unruh, D. K.; Ling, J.; Qiu, J.; Pressprich, L.; Baranay, M.; Ward, M.; Burns, P. C. *Inorg. Chem.* **2011**, *50*, 5509.
- (20) Ling, J.; Qiu, J.; Szymanowski, J. E. S.; Burns, P. C. *Chem.—Eur. J.* **2011**, *17*, 2571.
- (21) Ling, J.; Qiu, J.; Sigmon, G. E.; Ward, M.; Szymanowski, J. E. S.; Burns, P. C. *J. Am. Chem. Soc.* **2010**, *132*, 13395.
- (22) Unruh, D. K.; Baranay, M.; Baranay, M.; Burns, P. C. *Inorg. Chem.* **2010**, *49*, 6793.
- (23) Ling, J.; Wallace, C. M.; Szymanowski, J. E. S.; Burns, P. C. *Angew. Chem., Int. Ed.* **2010**, *49*, 7271.
- (24) Unruh, D. K.; Burtner, A.; Pressprich, L.; Sigmon, G. E.; Burns, P. C. *Dalton Trans.* **2010**, 39, 5807.
- (25) Sigmon, G. E.; Weaver, B.; Kubatko, K. A.; Burns, P. C. *Inorg. Chem.* **2009**, *48*, 10907.
- (26) Armstrong, C. R.; Nyman, M.; Shvareva, T.; Sigmon, G.; Burns, P. C.; Noavrotskt, A. *Proc. Natl. Acad. Sci. U.S.A.* **2012**, *109*, 1874.
- (27) Miro, P.; Pierrefixe, S.; Gicquel, M.; Gil, A.; Bo, C. *J. Am. Chem. Soc.* **2010**, *132*, 17787.
- (28) Vlasisavljevich, B.; Gagliardi, L.; Burns, P. C. *J. Am. Chem. Soc.* **2010**, *132*, 14503.

- (29) Forbes, T. Z.; McAlpin, J. G.; Murphy, R.; Burns, P. C. *Angew. Chem., Int. Ed.* **2008**, *47*, 2824.
- (30) Sigmon, G. E.; Unruh, D. K.; Ling, J.; Weaver, B.; Ward, M.; Pressprich, L.; Simonetti, A.; Burns, P. C. *Angew. Chem., Int. Ed.* **2009**, *48*, 2737.
- (31) Sigmon, G. E.; Ling, J.; Unruh, D. K.; Moore-Shay, L.; Ward, M.; Weaver, B.; Burns, P. C. *J. Am. Chem. Soc.* **2009**, *131*, 16648.
- (32) Mal, S. S.; Dickman, M. H.; Kortz, U. *Chem.—Eur. J.* **2008**, *14*, 9851.
- (33) Sheldrick, G. M. *SHELXTL*; Bruker AXS, Inc.: Madison, WI, 1996.
- (34) te Velde, G.; Bickelhaupt, F. M.; Baerends, E. J.; Guerra, C. F.; Van Gisbergen, S. J. A.; Snijders, J. G.; Ziegler, T. J. *Comput. Chem.* **2001**, *22*, 931.
- (35) Becke, A. D. *Phys. Rev. A* **1988**, *38*, 3098.
- (36) Perdew, J. P. *Phys. Rev. B* **1986**, *34*, 7406.
- (37) Perdew, J. P. *Phys. Rev. B* **1986**, *33*, 8822.
- (38) van Lenthe, E.; Baerends, E. J.; Snijders, J. G. *J. Chem. Phys.* **1993**, *99*, 4597.
- (39) van Lenthe, E.; Baerends, E. J.; Snijders, J. G. *J. Chem. Phys.* **1994**, *101*, 9783.
- (40) Pye, C. C.; Ziegler, T. *Theo. Chem. Acc.* **1999**, *101*, 396.
- (41) Klamt, A.; Schuurmann, G. *J. Chem. Soc., Perkin Trans.* **1993**, *2*, 799.
- (42) Allinger, N. L.; Yuh, Y. H.; Li, J. H. *J. Am. Chem. Soc.* **1989**, *111*, 8551.
- (43) Kelly, C. P.; Cramer, C. J.; Truhlar, D. G. *J. Phys. Chem. B* **2007**, *111*, 408.
- (44) Kelly, C. P.; Cramer, C. J.; Truhlar, D. G. *J. Phys. Chem. B* **2006**, *110*, 16066.
- (45) Poblet, J. M.; López, X.; Bo, C. *Chem. Soc. Rev.* **2003**, *32*, 297–308.
- (46) López, X.; Miró, P.; Carbó, J. J.; Rodríguez-Forteza, A.; Bo, C.; Poblet, J. M. *Theo. Chem. Acc.* **2011**, *128*, 393–404.
- (47) Janjua, M. R. S. A.; Amin, M.; Ali, M.; Bashir, B.; Khan, M. U.; Iqbal, M. A.; Guan, W.; Yan, L.; Su, Z.-M. *Eur. J. Inorg. Chem.* **2012**, 705–711.
- (48) Janjua, M. R. S. A.; Si, Z.-M.; Guan, W.; Liu, C.-G.; Yan, L.-K.; Song, P.; Maheen, G. *Aust. J. Chem.* **2010**, *63*, 836–844.
- (49) Gil, A.; Karhánek, D.; Miró, P.; Antonio, M. R.; Nyman, M.; Bo, C. *Chem.—Eur. J.* **2012**, *27*, 8340–8346.
- (50) Zhao, Y.; Truhlar, D. G. *J. Chem. Phys.* **2006**, *125* (194101), 1–18.
- (51) van Leeuwen, R.; Baerends, E. J. *Phys. Rev. A* **1994**, *49* (2421), 652.
- (52) Averkiev, B. B.; Mantina, M.; Valero, R.; Infante, I.; Kovaks, A.; Truhlar, D. G.; Gagliardi, L. *Theo. Chem. Acc.* **2011**, *129*, 657–666.
- (53) *TURBOMOLE V6.3 2011*, a development of University of Karlsruhe and Forschungszentrum Karlsruhe GmbH, 1989–2007, TURBOMOLE GmbH, since 2007; available from <http://www.turbomole.com>.
- (54) Schäfer, A.; Huber, C.; Ahlrichs, R. *J. Chem. Phys.* **1995**, *100*, 5829.
- (55) Eichkorn, K.; Dehnen, S.; Ahlrichs, R. *Chem. Phys. Lett.* **1998**, *284*, 287.
- (56) Eichkorn, K.; Weigend, F.; Treutler, O.; Ahlrichs, R. *Theo. Chem. Acc.* **1997**, *97*, 119.
- (57) Von Arnim, M.; Ahlrichs, R. *J. Comput. Chem.* **1998**, *19*, 1746.
- (58) Schäfer, A.; Klamt, A.; Sattel, D.; Lohrenz, J. C. W.; Eckert, F. *Phys. Chem. Chem. Phys.* **2000**, *2*, 2187.
- (59) Lu, T.; Chen, F. *J. Comput. Chem.* **2012**, *33*, 580.
- (60) Cotton, S. *Lanthanide and Actinide Chemistry*, 2nd ed.; Wiley: 2006.
- (61) Leroy, F.; Miro, P.; Poblet, J. M.; Bo, C.; Avalos, J. B. *J. Phys. Chem. B* **2008**, *112*, 8591.
- (62) Guan, W.; Yan, L. K.; Su, Z. M.; Wang, E. B.; Wang, X. H. *Int. J. Quantum Chem.* **2006**, *106*, 1860.
- (63) Miro, P.; Bo, C. *Inorg. Chem.* **2012**, DOI: 10.1021/ic300029d.
- (64) Courcot, B.; Bridgeman, A. J. *J. Phys. Chem. A* **2009**, *113*, 10540.
- (65) Essayem, N.; Holmqvist, A.; Gayraud, P. Y.; Vedrine, J. C.; Ben Taarit, Y. *J. Catal.* **2001**, *197*, 273.
- (66) Bader, R. F. W. *Atoms In Molecules: A Quantum Theory*; Clarendon Press: Oxford, 1990.
- (67) Bader, R. F. W. *J. Phys. Chem. A* **1998**, *102*, 7314.
- (68) Bianchi, R.; Gervasio, G.; Marabello, D. *Inorg. Chem.* **2000**, *39*, 2360.